



## SPECIAL ISSUE RESEARCH ARTICLE

# Test method for evaluating the photocytotoxic potential of fluorescence imaging products

Shruti Vig<sup>1</sup> | Brandon Gaitan<sup>1,2</sup> | Lucas Frankle<sup>1</sup> | Yu Chen<sup>3</sup> | Rosalie Elespuru<sup>2</sup> | T. Joshua Pfefer<sup>2</sup> | Huang-Chiao Huang<sup>1</sup>

<sup>1</sup>Fischell Department of Bioengineering, University of Maryland, College Park, Maryland, USA

<sup>2</sup>Center for Devices and Radiological Health, US Food and Drug Administration, Silver Spring, Maryland, USA

<sup>3</sup>Department of Biomedical Engineering, University of Massachusetts, Amherst, Massachusetts, USA

## Correspondence

Huang-Chiao Huang, Fischell Department of Bioengineering, University of Maryland, College Park, MD, USA.

Email: [hchuang@umd.edu](mailto:hchuang@umd.edu)

## Funding information

NSF-FDA, Grant/Award Number: 2037815; MPower Fellowship; Clark Doctoral Fellowship; University of Maryland ASPIRE Fellowship

## Abstract

Various fluorescence imaging agents are currently under clinical studies. Despite significant benefits, phototoxicity is a barrier to the clinical translation of fluorophores. Current regulatory guidelines on medication-based phototoxicity focus on skin effects during sun exposure. However, with systemic and local administration of fluorophores and targeted illumination, there is now possibility of photochemical damage to deeper tissues during intraoperative imaging procedures. Hence, independent knowledge regarding phototoxicity is required to facilitate the development of fluorescence imaging products. Previously, we studied a cell-free assay for initial screening of reactive molecular species generation from fluorophores. The current work addresses a safety test method based on cell viability as an adjunct and a comparator with the cell-free assay. Our goal is to modify and implement an approach based on the in vitro 3T3 neutral red uptake assay of the Organization for Economic Co-Operation and Development Test Guideline 432 (OECD TG432) to evaluate the photocytotoxicity of clinically relevant fluorophores. These included indocyanine green (ICG), proflavine, methylene blue (MB), and IRDye800, as well as control photosensitizers, benzoporphyrin derivative (BPD) and rose bengal (RB). We performed measurements at agent concentrations and illumination parameters used for clinic imaging. Our results aligned with prior studies, indicating photocytotoxicity in RB and BPD and an absence of reactivity for ICG and IRDye800. DNA interactive agents, proflavine and MB, exhibited drug/light dose–response curves like photosensitizers. This study provides evidence and insights into practices useful for testing the photochemical safety of fluorescence imaging products.

## KEYWORDS

fluorescence imaging, fluorescence imaging agents, neutral red uptake (NRU) assay, OECD TG432, photocytotoxicity

**Abbreviations:** BPD, benzoporphyrin derivative; FBS, fetal bovine serum; FGS, fluorescence-guided surgery; ICG, indocyanine green; MB, methylene blue; NRU, neutral red uptake; PDT, photodynamic therapy; RB, rose bengal; RMS, reactive molecular species.

This article is part of a Special Issue dedicated to the topic of Critical Issues and Recent Progresses in Clinical Translation of Photomedicine.

This is an open access article under the terms of the [Creative Commons Attribution-NonCommercial-NoDerivs](https://creativecommons.org/licenses/by-nc-nd/4.0/) License, which permits use and distribution in any medium, provided the original work is properly cited, the use is non-commercial and no modifications or adaptations are made.

© 2023 The Authors. *Photochemistry and Photobiology* published by Wiley Periodicals LLC on behalf of American Society for Photobiology.

## INTRODUCTION

Fluorescence imaging can aid in the visualization of critical nerves, vascular structures, tumor margins, and metastases. This optical tool is minimally invasive, real-time, and provides a better resolution for detection compared to naked eye, and thus is being increasingly accepted by clinicians.<sup>1,2</sup> Fluorescent agents can be broadly classified as non-targeted, metabolic, and molecular-targeted agents.<sup>3</sup> For example, indocyanine green (ICG) and fluorescein are non-targeted fluorescent agents used for retinal angiography<sup>4,5</sup> and fluorescence-guided surgery (FGS).<sup>6,7</sup> Methylene blue (MB) has been studied for tumor imaging<sup>8–11</sup> and sentinel lymph node mapping for axillary staging in breast cancer.<sup>12,13</sup> Proflavine's ability to bind to cell nuclei offers a proper assessment of nuclear architecture and grading of oral carcinoma.<sup>14</sup> Molecular-targeted approaches have also been explored to improve the selectivity of fluorescent agents. For example, conjugation of IRDye800CW to tumor-targeting moieties, such as antibodies, is under clinical investigations for FGS of head and neck cancer<sup>15</sup> and visualization of other cancers.<sup>16</sup> Many fluorescent agents can also generate cytotoxic reactive molecular species (RMS), making them ideal for combined optical imaging and phototherapy applications. For instance, MB is being evaluated for real-time visualization of ureters during abdominal and laparoscopic surgeries,<sup>17,18</sup> identification of enlarged thyroid and parathyroid glands,<sup>19,20</sup> as well as fluorescence imaging and phototherapy of localized cutaneous amyloidosis and toenail onychomycosis.<sup>21–23</sup> ICG has also been studied for photodynamic therapy (PDT) and is currently being assessed for usage in periodontal disease and with diabetic patients having peri-implantitis.<sup>24,25</sup>

The safe use of light-emitting devices for medical applications is addressed by well-established international consensus standards.<sup>26,27</sup> Yet, the use of such devices in combination with fluorophores is not satisfactorily addressed in these documents. One potential barrier to the clinical translation of products involving optical devices and fluorophores is normal tissue phototoxicity. When exposed to light at specific wavelengths, fluorophores can produce photochemical reactions that cause phototoxicity.<sup>28</sup> These photoreactive agents often undergo electronic excitation and produce RMS like singlet oxygen, superoxide, hydroxyl radicals, and hydrogen peroxide, which can cause cellular and tissue damage through Type I and Type II photochemical reactions.<sup>29</sup> Type I and II reactions require oxygen as a reagent for the formation of RMS.<sup>30</sup> Type I reactions lead to the formation of hydroxyl radicals, hydrogen peroxide, and superoxide ions. Type II reactions involve an energy transfer reaction between the photoactivated agent and molecular oxygen, leading to the formation

of singlet oxygen. Thus, given the fluorophore potential to cause unintentional damage to a patient through various mechanisms, it is important to evaluate their phototoxicity to ensure safe clinical application. Independent of the nature of toxicity generated by the photoactivation of these fluorophores, the outcomes are cellular alterations or lethality. While studies have focused on developing test methods for detecting phototoxicity, there is still a dearth of standardized test methods for the photochemical safety of clinical fluorescence imaging products.

The neutral red (3-amino-7-dimethyl-2-methyl phenazine hydrochloride) uptake (NRU) assay was developed in 1985 by Borenfreund and Puerner, as a cell viability assay based on the ability of cells to incorporate and bind to neutral red dye (NR).<sup>31</sup> NR is a weak cationic dye with a net charge close to zero. It penetrates cells by non-ionic diffusion at physiological pH and accumulates intracellularly in lysosomes.<sup>32</sup> Inside the lysosomes exists a proton gradient, due to which the dye becomes charged and is retained. The NRU assay allows the assessment of membrane permeability and lysosomal activity, making it possible to differentiate between viable, damaged, and dead cells. The assay was an early attempt to establish a more quantitative, reproducible, inexpensive, and sensitive method for in vitro toxicity screening compared to other subjective methods (like morphological inspection).<sup>31</sup> The assay has been adapted to assess cytotoxicity and phototoxicity screening of chemicals/products in vitro.<sup>33,34</sup> Several validation studies have been set up for the NRU assay.<sup>35,36</sup> In 2000, the NRU test on BALB/c 3T3 mouse fibroblasts to assess phototoxicity was accepted in the EU. In 2004, the Organization for Economic Cooperation and Development (OECD) described a method to evaluate photocytotoxicity in the OECD TG 432 guideline.<sup>37</sup> In 2013, EURL ECVAM (European Commission Joint Research Centre) published regulatory recommendations on the use of the 3T3 NRU assay to predict acute oral toxicity of chemicals.<sup>38</sup>

The Center for Drug Evaluation and Research (CDER) and the Center for Biologics Evaluation and Research (CBER) of the U.S. Food and Drug Administration (FDA) recommend phototoxic assessment of agents that absorb light within the range of natural sunlight (290–700 nm).<sup>39</sup> The International Council for Harmonization of technical requirements for pharmaceuticals for human use (ICH) S10 guidelines emphasize the need to develop initial in vitro phototoxicity tests before carrying out clinical trials. ICH S10 provides guidelines on the initial photochemical properties of agents to be considered for phototoxic testing. For an agent to demonstrate potential phototoxicity, it should (a) absorb light within the wavelength range of 290–700 nm (sunlight spectrum), (b) generate RMS following absorption of UV-visible light, and (c) showcase

a molar extinction coefficient greater than 1000 L/mol/cm. FDA currently accepts the in vitro 3T3 NRU assay for evaluating the phototoxicity of drugs.<sup>37</sup> OECD TG432 guidelines recommend using a solar simulator to mimic sunlight exposure at a set non-cytotoxic irradiation dose of 5 J/cm<sup>2</sup> at 1.7 mW/cm<sup>2</sup> as an acceptable light source for 3T3-NRU phototoxicity testing. While photosensitivity due to solar exposure has historically been a primary concern, there is now the potential for photochemical damage to internal organs and tissues during intraoperative imaging procedures. Furthermore, the emerging NIR fluorophores absorb irradiations at high fluence targeted wavelengths that may be beyond the sunlight spectrum. Thus, independent knowledge regarding RMS generation and related photocytotoxicity for existing and emerging fluorescent dyes at doses and exposure levels used for clinical imaging is needed to streamline product development and regulations for clinical applications.

In this study, we used a modified phototoxicity assessment strategy based on OECD TG432 guidelines to assess the photocytotoxicity of contrast-enhanced fluorescence imaging products for a range of concentrations and illuminations within and above the clinical range used for diagnostic imaging. Instead of using solar radiation for these experiments, the NRU assay was performed at concentration ranges and illumination parameters used in the clinic for diagnostic imaging to establish a dose–response curve for each contrast agent. As outlined in the OECD TG432 guidance document, mean photo effect (MPE) was calculated for fluorophore concentration ranges at tested radiant exposures ( $H_e$ ) [J/cm<sup>2</sup>], which is defined as a product of laser irradiance and time. In addition to providing insights into assessing photocytotoxicity generated by fluorescence imaging products and the limitations of the assay approach, this study highlights potential best practices for preclinical safety assessment of contrast-enhanced fluorescence imaging products.

## MATERIALS AND METHODS

### Overview

In this study, the 3T3 NRU phototoxicity assessment<sup>37</sup> was modified by: (a) expanding the recommended illumination wavelength range beyond 290–700 nm to accommodate long wavelength contrast agents for phototoxicity testing; (b) establishing the dose–response curve for agent concentrations from available literature and OECD-recommended concentrations to account for variance in photocytotoxicity to determine potential safety thresholds for fluorophores; (c) evaluating photocytotoxicity generated at clinically used illumination levels—excitation

wavelengths, irradiance, and radiant exposure ( $H_e$ ) using laser diodes, as opposed to irradiation with a broadband solar simulator suggested in current guidelines. The study encompassed four phases (1) utilize agent concentrations, optical exposure wavelengths, and  $H_e$  levels from available literature on clinical and animal studies summarized in our previous study and Table 1; (2) obtain experimental data with each fluorophore using the NRU assay; (3) analyze the resultant dose–response curves to assess prediction model values (MPE) for different fluorophore products; and (4) compare the results with published literature and assess overall performance and limitations of the assay. The existing method for testing medication-based phototoxicity suggested by the OECD guidelines is summarized in Figure S1.

### Cell culture

BALB/c 3T3 clone A31 (ATCC) cells were cultured following recommendations from the OECD 432 guidelines.<sup>37</sup> Briefly, cells were cultured in T-75 flasks (Cell Treat) in a 37°C and 5% CO<sub>2</sub> incubator until they reached 80%–90% confluency. Dulbecco's modified eagle's medium (DMEM) (ATCC) supplemented with 10% fetal bovine serum (FBS) (Gibco), 1% penicillin–streptomycin (Corning) were used to maintain the cells. The medium was changed every 48 h. BALB/c 3T3 cells were confirmed to be mycoplasma free using the Mycoalert™ Plus mycoplasma detection kit (Lonza). To optimize the cell seeding for phototoxicity evaluation, BALB/c 3T3 cells were plated over a range of cell seeding numbers (from  $1.0 \times 10^3$  to  $1.2 \times 10^5$  cells per well) in 96-well tissue culture plates (Southern Labware). After 48 h, an MTT (3-(4,5-dimethylthiazol-2-yl)-2,5-diphenyltetrazolium bromide) assay (Invitrogen) was performed following the vendor protocol. Briefly, 3T3 cells were incubated with 0.25 mg/mL of MTT for 1 h. The formazan crystals formed were solubilized in 100% DMSO, and the absorbance was measured at 570 nm using a spectrophotometer (Synergy Neo2; Biotek) (Figure S2).

### Fluorophore concentrations and illumination levels

RMS generation by contrast agent depends on the excitation spectrum and  $H_e$  of the illumination source in addition to the concentration of the agent. This study focused on the phototoxic potential of fluorescence imaging products at clinically relevant concentrations and exposure parameters. The literature review identified appropriate parameters for testing each contrast agent. Fluorophores were tested for concentrations ranging from

**TABLE 1** Literature review summary on the clinical use of imaging fluorophores tested in the study: concentration, excitation wavelength, and irradiance.

Fluorophore	Model	Use case	Concentration	Excitation wavelength (nm)	Irradiance	Imaging time	Citation
ICG	Human	Lymphatic imaging	0.2 mL injected	760	NA	NA	Unno et al. <sup>81</sup>
	Human	Lymphatic imaging	1 mL of 0.5% ICG injected	750–800	NA	30 min	Takeuchi et al. <sup>82</sup>
	Human	Blood conc. of ICG	5–30 mg/L in plasma	805	NA	NA	Imai et al. <sup>83</sup>
	NA	Instrument review	NA	785	1.9 mW/cm <sup>2</sup>	NA	Zhu et al. <sup>42</sup>
	Human	Lymph node imaging	1 mL injected	760	4 mW/cm <sup>2</sup>	15 min	Tagaya et al. <sup>41</sup>
IRDye800	Human	Head and neck surgery	5.2–130 mg injected	775	NA	NA	Gao et al. <sup>84</sup>
	Human	Glioblastoma imaging	50–100 mg injected	NA	NA	NA	Miller et al. <sup>45</sup>
	NA	Instrument review	NA	780	3–30 mW/cm <sup>2</sup>	NA	D'Souza et al. <sup>46</sup>
	Human	Oral cancer imaging	0.01% (w/v)	455	NA	NA	Shin et al. <sup>48</sup>
Proflavine	Human	Oral cancer imaging	0.01%	455	NA	3–15 min	85
	Human	Imaging of Barrett's related neoplasia	0.01% (w/v)	435/500	8.2 and 14.9 mW	NA	Tang et al. <sup>47</sup>
MB	Human	Intravenous bio-availability	600–2000 ng/mL in blood	NA	NA	NA	Stefano et al. <sup>43</sup>
	Swine	Uterine imaging	0.1 mg/kg injected	670	2.5 mW/cm <sup>2</sup>	NA	Matsui et al. <sup>44</sup>
	Human	Uterine imaging	0.25–1 mg/kg injected	670	1.08 mW/cm <sup>2</sup>	> 5 min	Verbeek et al. <sup>40</sup>
	Human	Breast cancer imaging	1 mg/kg injected	670	1.08 mW/cm <sup>2</sup>	NA	Tummers et al. <sup>10</sup>

Abbreviations: ICG, indocyanine green; MB, methylene blue.

Source: Adapted from our previous study.<sup>56</sup>

0  $\mu\text{M}$  (negative control) to approximately twice the concentration used in the clinic for imaging. A brief literature review summary on the illumination parameters of the contrast agents can be found in Table 1. The exposure time depends on acquiring adequate fluorescence signal during intraoperative imaging of tissues.<sup>40,41</sup> The 2 $\times$  concentration range used for each agent was based on parameters reported in the literature, like human blood plasma levels, pharmacokinetics data after intravenous injection, and clinical studies on using the test agents for FGS. The 2 $\times$  ICG concentration range was based on the blood plasma values found in human subjects. The illumination parameters ( $H_e$  and excitation wavelength) for ICG were derived from values used for fluorescent-guided surgery.<sup>42</sup> The concentration range of 1–7.5  $\mu\text{M}$  for MB was used based on the pharmacokinetics data acquired after oral dose of 100 mg in human subjects.<sup>43</sup> The  $H_e$  (0–6 J/cm<sup>2</sup>) was determined through camera exposure time required during fluorescence-guided identification of ureters using MB.<sup>44</sup> The 2.5–20  $\mu\text{M}$  concentration range for IRDye800 was based on clinical studies using IRDye800 as contrast agent for FGS.<sup>45,46</sup> The  $H_e$  range was based on current imaging devices and the likely duration of imaging during surgery.<sup>46</sup> For proflavine, concentration range of 1.5–12  $\mu\text{M}$ ,  $H_e$  range of 0–6 J/cm<sup>2</sup>, and excitation wavelength of 445 nm were based on human trials using proflavine as an imaging agent to detect oral cancer.<sup>47,48</sup> Rose bengal (RB) and BPD were included as positive controls since they are known to generate RMS after photoactivation and are used as photodynamic agents.<sup>49,50</sup> The BPD concentration range of 0–10  $\mu\text{M}$  and  $H_e$  was based on in vivo studies where 0.5 mg of the agent was intravenously administered in rabbits.<sup>51</sup> RB concentrations (0–10  $\mu\text{M}$ ) and exposure levels ( $H_e$ , 0.2 J/cm<sup>2</sup>) were selected to achieve similar dose levels as BPD to compare results. The concentration range of test agents was increased up to 100  $\mu\text{g/mL}$  per OECD 432 guidelines to test the photocytotoxicity generated at higher concentrations to determine potential

safety thresholds for the fluorophores. The  $H_e$  and illumination wavelengths were determined from clinical studies using contrast agents for FGS, camera exposure times, and imaging duration during surgery. The concentration ranges, excitation wavelengths, irradiance, and  $H_e$  used in the study are summarized in Table 2.

## Optical exposure system setup and validation

A custom setup was developed to illuminate 4 wells simultaneously in a 2 $\times$ 2 square format within a 96-well plate (Figure 1). The bottom-up exposure setup comprised a laser diode controller (Thorlabs, Inc.), a laser diode, an achromatic collimating lens ( $f = 50$  mm), a 45° mirror, and a 20° square diffuser (ED1-S50-MD) (Thorlabs, Inc.). The laser light was collimated, reflected 90°, passed through a diffuser, and projected onto a 0.5" thick black marine board plate (Onlinemetals) with a 1"  $\times$  1" aperture to allow illumination of the four wells. Laser diodes (Thorlabs, Inc.) with the following central wavelengths were used: 520 nm (RB, LP520-SF15), 785 nm (ICG/IRDye800, L785H1), 660 nm (MB, L660P120), 685 nm (BPD, HL6750MG), and 450 nm (PL450B, Proflavine). Power measurements were taken at the set current (mA) used during treatment to ensure uniform power distribution during laser exposure. An actuated iris diaphragm (Thorlabs, SM1D12) was attached to the power meter sensor (model PMD100D, Thorlabs, Inc.) sized at 1:1 (area of diaphragm:active area of the power meter sensor—1.31 cm<sup>2</sup>) and placed above the 1"  $\times$  1" aperture to measure the output power at each of the four well locations. The location of each well during illumination was marked on the board plate to ensure that measurements were taken from a fixed location. Irradiance (mW/cm<sup>2</sup>) was calculated by dividing the laser diode power readings by the active sensor area. The same procedure was carried out on all the laser diodes.

**TABLE 2** Summary of the concentration range, excitation wavelength (laser diodes), irradiance, and  $H_e$  (maximum tested) values used in our study for the modified NRU assay.

Fluorophore	Extended conc. range ( $\mu\text{M}$ )-OECD	Conc. range ( $\mu\text{M}$ )-imaging (2 $\times$ )	Excitation wavelength (nm)	Irradiance (mW/cm <sup>2</sup> )	Exposure time (s)	Max tested radiant exposure, $H_e$ (J/cm <sup>2</sup> )
ICG	0–175	6.5–26	785	10	600	6
IRDYE800	0–75	2.5–20	785	10	600	6
Proflavine	0–1000	0.5–12	450	4.2	143	0.6
MB	0–500	1–7.5	660	10	600	6
Benzoporphyrin derivative	0–10	0.5–1	685	7.2	28	0.2
Rose bengal	0–10	0.5–2	520	1.6	125	0.2

Abbreviations: ICG, indocyanine green; MB, methylene blue.



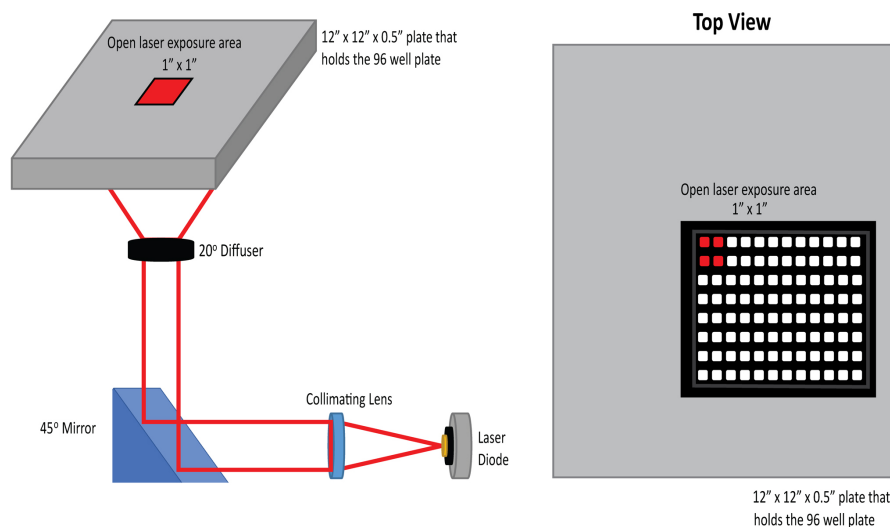


**FIGURE 1** Schematic of the laser exposure system. A laser diode was coupled to a collimating lens; the beam was then reflected at 90° using a mirror and passed through a 20° diffuser. The light was subsequently passed through a 1" × 1" square aperture, where it exposed the bottom of a 96-well plate. The top view shows the irradiation format of the samples plated on the 96-well plate.

## Modified neutral red uptake (NRU) assay

For testing,  $1.0 \times 10^4$  BALB/c 3T3 A31 clone cells were plated in 100- $\mu$ L complete growth medium per well in two 96-well, black-walled, clear flat bottom microtiter plates (Southern Labware). The cells were allowed overnight attachment at 37°C in a humidified atmosphere containing 5% CO<sub>2</sub>. The 96-well plates were labeled as irradiation (IRR) or NO IRR. On Day 1, a fresh fluorophore solution was prepared in DMSO or HBSS based on the solubility of the agent. Eight different testing concentrations were prepared per fluorophore. Each testing concentration had six replicates per plate (Figure S3 for the sample plating layout). For testing, the wells were washed with 100  $\mu$ L of HBSS, followed by adding 100  $\mu$ L of the test fluorophore concentration, and incubated for 60 min in both plates. The no-treatment control wells contained 100  $\mu$ L of the solvent control (0.1% DMSO in HBSS or HBSS only). After 60 min, the IRR plate was illuminated to achieve the desired  $H_e$  at set irradiance (Table 2). For  $H_e$  of 1 J/cm<sup>2</sup>, the wells were irradiated in 60/4 radiations (total wells/number of wells illuminated with the 2 × 2 exposure area at a time). Exposure time for the IRR group varied depending on the test  $H_e$  for each agent. The NO IRR plate was stored in the dark at room temperature while illuminating the IRR plate. For testing at higher  $H_e$  (6 J/cm<sup>2</sup>), the experiment was carried out using four instead of two 96-well plates. To minimize the exposure of cells to room temperature for prolonged time intervals (<35 min) during illumination, (i) two instead of eight fluorophores concentrations, with dark and solvent controls, were tested per plate; (ii) four replicates per condition were tested at higher  $H_e$ . For  $H_e$  of 6 J/cm<sup>2</sup>, 12 of 24 wells (IRR group

only) per plate were irradiated in 12/4 irradiations. After illumination, the solution was removed, and the cells were washed twice with 200  $\mu$ L of HBSS and incubated with the cell growth medium for 24 h. The NRU assay was performed on Day 2 using the neutral red assay kit (Abcam). NRU assay is based on detecting viable cells via the uptake of the dye-neutral red that stains lysosomes in viable cells. Briefly, treated cells were incubated with 150  $\mu$ L of the 1× neutral red solution for 3 h based on the parameters optimized in a previous study.<sup>52</sup> The cells were washed with 200  $\mu$ L of the wash solution (1× PBS). Consequently, cells are incubated with 200  $\mu$ L of solubilization solution to release the incorporated neutral red dye under acidified-extracted conditions. The absorbance of NR dye in the solubilization solution was measured at 540 nm using a spectrophotometer (Synergy Neo2; BioTek). The modified method for photocytotoxicity assessment of fluorophore products is summarized in Figure 2. Surviving cells were normalized to the no treatment (solvent controls) on each plate. Further analysis on endpoint readout of NRU assay is depicted in Figure S3. To determine if the absorbance spectrum of the test fluorophore affects the NRU absorbance spectrum during phototoxicity evaluation, the cells were incubated with the fluorophores on Day 1, for about 1.5 h, considering the time for fluorophore incubation and illumination. Control wells were treated with 100  $\mu$ L of HBSS. After incubation, 3T3 cells were washed with HBSS and incubated with media overnight. For the fluorophores-alone group, cells were incubated with fluorophores overnight. As described previously, the NRU assay was performed on Day 2, and the absorbance spectrum was recorded using the spectrophotometer (Synergy Neo2; BioTek).

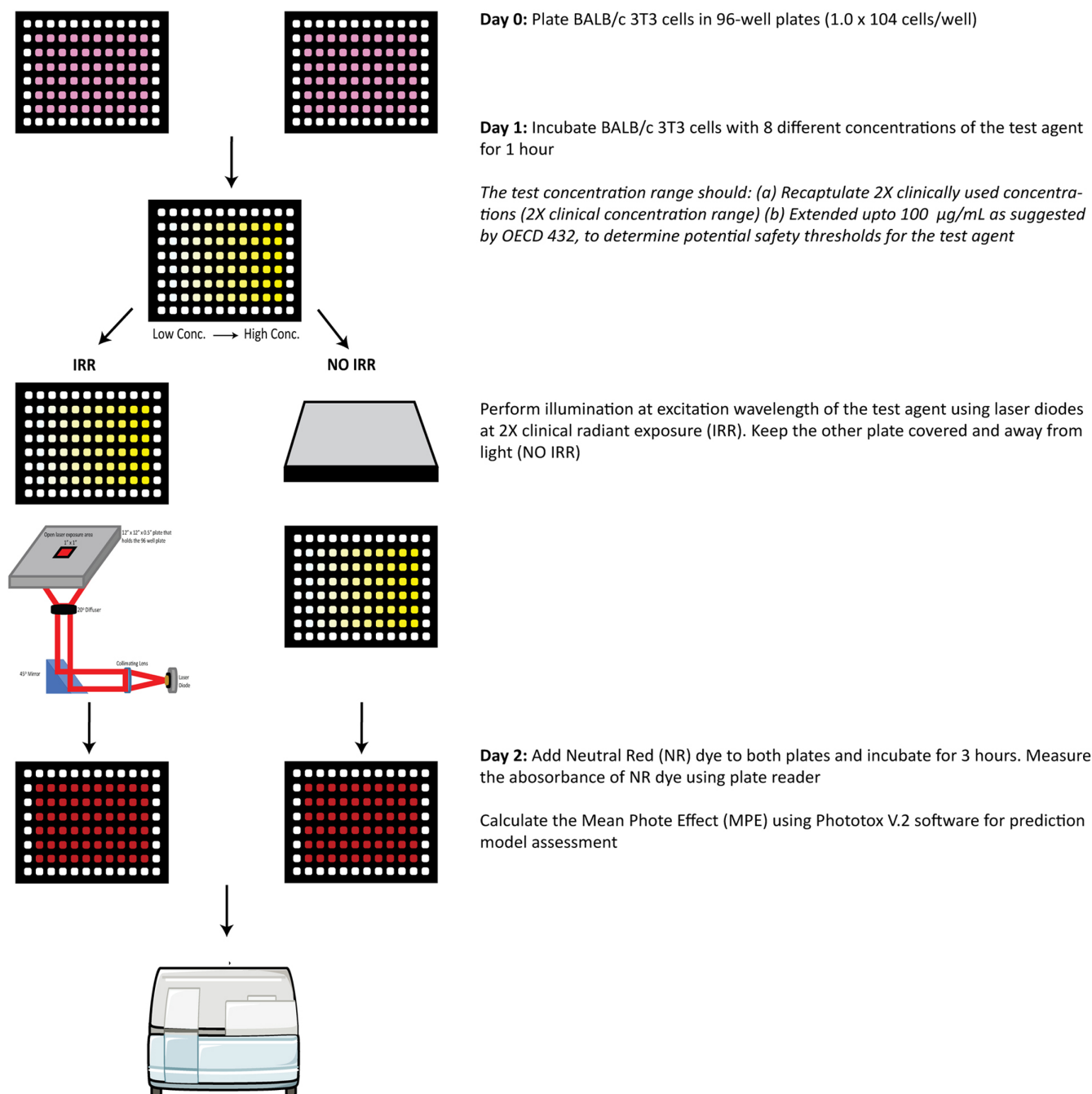


**FIGURE 2** Modified test method for assessing phototoxicity of fluorophore products activated by lasers at specific wavelengths and illumination parameters. BALB/3T3 cells are exposed to different concentrations of the fluorophore of interest. To study the effect of tissue phototoxicity caused during diagnostic imaging, the 96-well plate is exposed to 2× illumination parameters used clinically for fluorophore excitation. NRU assay is performed on Day 2, and the absorbance values of uptake NR dye are recorded at 540 nm using a plate reader. IRR, irradiation; NRU, neutral red uptake.

## Data analysis

The concentration-dependent cytotoxic responses in the presence of light (IRR) and in the absence of light (NO IRR) were determined in the NRU assay. For data evaluation, the prediction value recommended in OECD 432, the MPE, was calculated using Phototox version 2.0 software.<sup>37</sup> The MPE prediction model was proposed by

Holzhütter et al.<sup>53</sup> and has been used for the phototoxicity assessment of chemical agents.<sup>54</sup> MPE is calculated based on a comparison of the IRR and NO IRR response curves on a set of commonly tested concentration ranges ( $i = 1, \dots, n$ ) of IRR and NO IRR curves (Equation 1).

$$\text{MPE} = \frac{\sum_{i=1}^n w_i \text{PE}_{c_i}}{\sum_{i=1}^n w_i} \quad (1)$$

where photo-effect ( $PE_c$ ) at any concentration  $C$  is a product of dose-effect ( $DE_c$ ) and the response effect ( $RE_c$ ). The dose-effect ( $DE_c$ ) was calculated as

$$DE_c = \left| \frac{C/C^* - 1}{C/C^* + 1} \right|$$

$C^*$  represents the concentration at which the IRR response equals the NO IRR response at concentration  $C$ . If  $C^*$  cannot be determined because the response of the IRR curve is higher or lower than the NO IRR, the  $DE$  is set to 1 at that concentration. The response effect ( $RE_c$ ) at concentration  $C$  represents the difference between responses observed in the absence and presence of light, that is,

$$RE_c = [R_c(\text{NO IRR}) - R_c(\text{IRR})] / 100$$

The weighing factors  $w_i$  were determined by the highest response value, that is,  $w_i = \text{MAX} [R_i(\text{IRR}), R_i(\text{NO IRR})]$ . The MPE was subsequently obtained by averaging across all  $PE_c$  values. For calculating MPE using the Phototox software, the set of concentration-response values was input into the software. Fitting the curve to the data by non-linear regression was performed using the Phototox V.2 software. A bootstrap resampling (i.e., selecting data points randomly with replacements) was performed to assess the influence of data variability on the fitted curve. Based on the MPE values, the fluorophore product at each tested  $H_c$  level was estimated to be non-phototoxic, equivocal-phototoxic, or phototoxic, using the standard in OECD 432. An example of the detailed calculation for estimating MPE values can be found in Figures S4 and S5.

## Statistical analysis

The cell viability response was calculated using the normalized average absorbance values of replicates obtained using the NRU assay. The cell viability was presented as mean  $\pm$  standard error of the mean (SEM). Statistical analysis was conducted using GraphPad PRISM version 9.0.2. Data were analyzed using a paired Student's  $t$ -test. A value of  $p \leq 0.05$  was considered statistically significant. All experiments were repeated at least thrice to assess repeatability ( $n \geq 3$ ).

## RESULTS

### Validation of illumination system and NRU assay

To investigate variation in irradiance during the illumination experiments for photocytotoxicity evaluation,

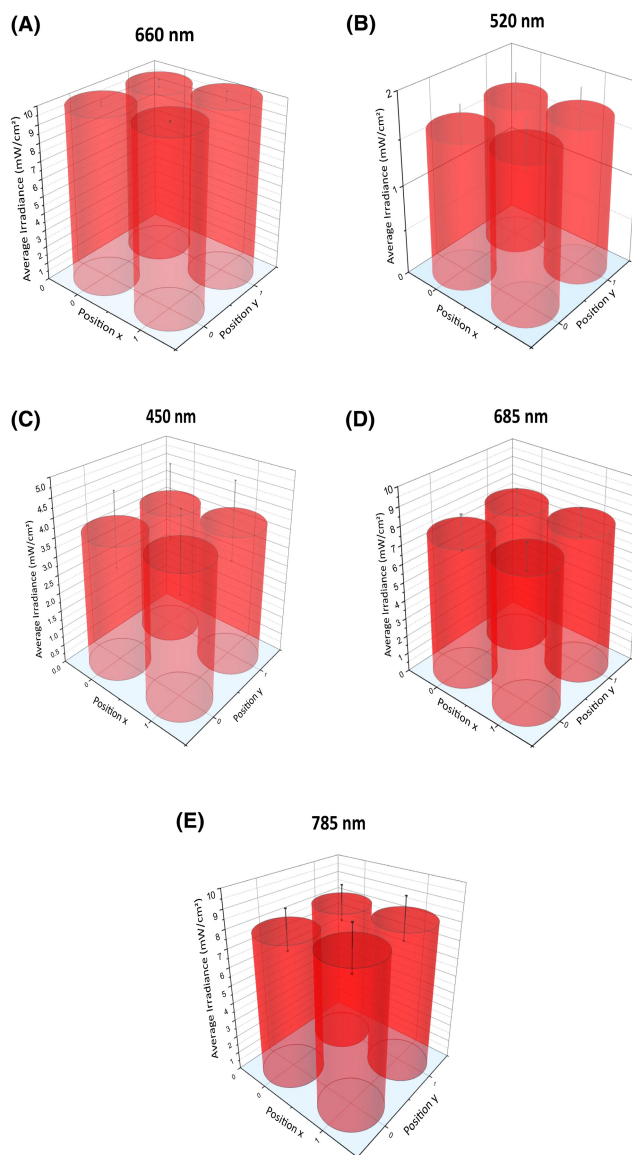


**FIGURE 3** Laser exposure system validation for used laser diodes. Individual average irradiance readings of four wells exposed to laser diode through the 1"  $\times$  1" aperture for (A) 660nm, (B) 520nm, (C) 450nm, (D) 685nm, and (E) 785nm laser diodes; plots show less than 10% variation in irradiance among the wells ( $n = 3$ ).

irradiance of the laser diode at the 2  $\times$  2 illumination area was recorded. Figure 3 shows the average irradiance recorded using the power sensor during the illumination of wells. The actuated iris diaphragm, sized at 1:1, was placed above the four open exposure areas at each well location. The average power distribution among the four well-open areas exposed to the laser was consistent for the adjacent wells during treatment. The variance in output was calculated to be less than 10% between different repeats during illumination experiments.

NRU assay involves absorbance measurement of neutral red as the endpoint to quantify cell viability. Since the test fluorophores are also dyes, we investigated the



interference of fluorophore absorbance with the endpoint NR dye absorbance. In Figure 4A–F, we present the absorbance spectra of the NR dye after the treatment of cells with a test fluorophore. The absorption peak of NR dye can be seen at 540 nm in the wells treated with HBSS only [NRU(3T3 + HBSS)]. There was minimal to no crossover with the NR dye for most fluorophores tested, such as ICG, IRDye800, MB, and BPD. The exception

was RB, MB, and Proflavine (to some extent). To further assess whether the residual fluorophore in the wells (due to fluorophore uptake or incomplete HBSS washes) affected the NR dye absorption reading, the absorbance spectra of NR dye were recorded post-fluorophore incubation [NRU (3T3 + Test Fluorophore)]. No change in the NR absorbance spectrum was observed due to fluorophore incubation between the NRU (3T3 + HBSS)

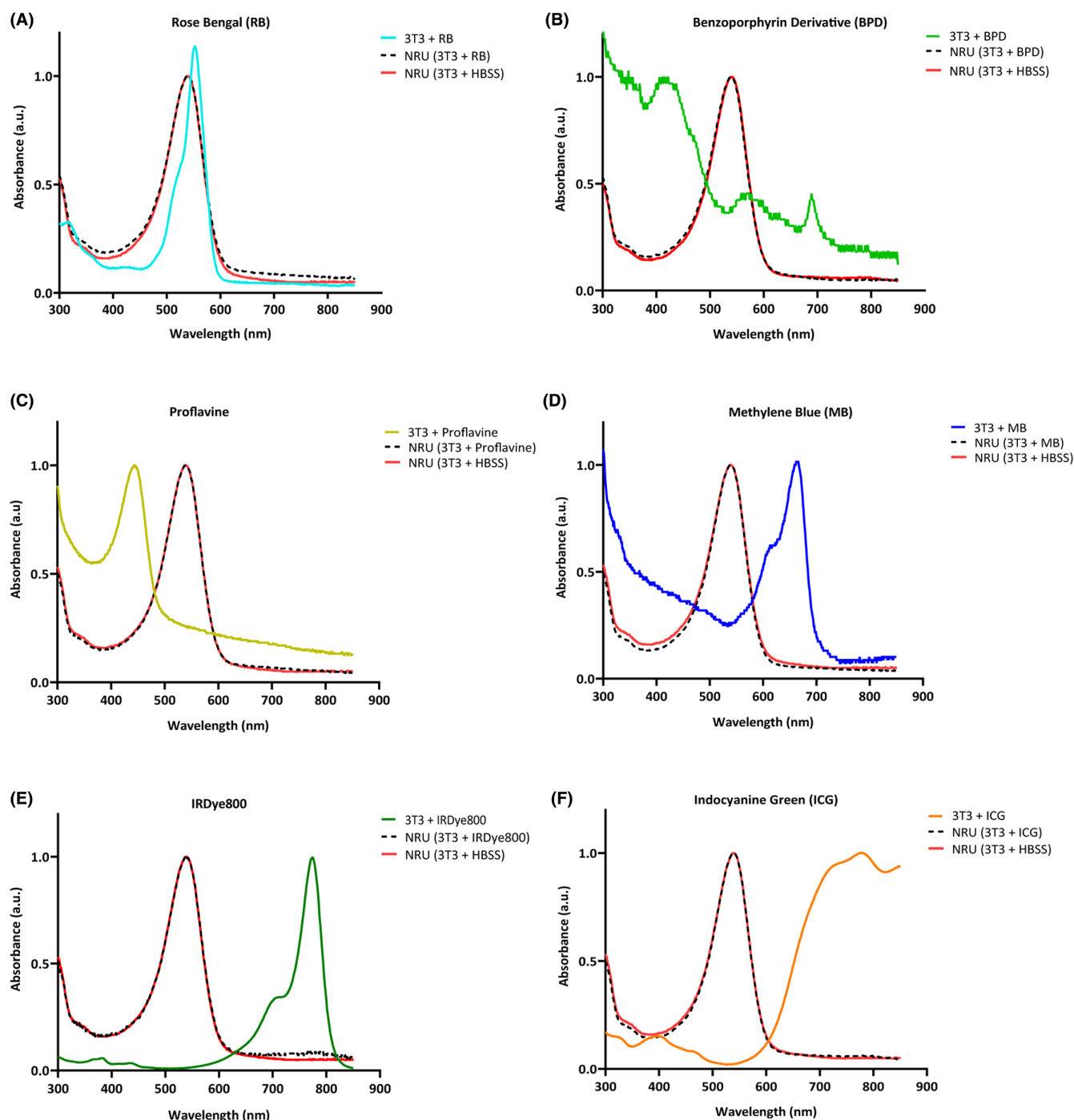


**FIGURE 4** Comparative absorbance spectra of NR dye with tested fluorophores. Absorbance spectra were measured for (A) RB, (B) BPD, (C) Proflavine, (D) MB, (E) IRDye800, and (F) ICG. Plots demonstrate the peak-normalized absorbance of tested fluorophores incubated with 3T3 cells, NR dye post-incubation of cells with fluorophores, and NR dye post-incubation with solvent. NRU: neutral red uptake.

and the NRU (3T3 + Test Fluorophore) groups for all the test fluorophores. Thus, it was concluded that the fluorophore absorption overlap with NR dye does not affect the NR absorbance in the study.

### Evaluation of the photocytotoxicity using the modified NRU assay

The cell viability curves were obtained using the NRU assay at test concentrations, clinically relevant excitation wavelengths, and  $H_e$  for all the tested fluorophores

in this study. Dose-response curves for the positive controls at the extended concentration ranges recommended by OECD for solar light-activated studies, along with 2× of clinically used concentrations, are shown in Figure 5. For the positive control, RB, a concentration-dependent decrease in cell viability was observed at the  $H_e$  of 0.2 J/cm<sup>2</sup>. A concentration-dependent decrease in cell viability was also observed beyond 1 μM in the NO IRR group due to the intrinsic toxicity of the RB.<sup>55</sup> The agent shows light-independent cytotoxicity in the 1–10 μM dose range. A similar expected trend was observed for BPD products at  $H_e$  as low as 0.2 J/cm<sup>2</sup>, indicating significant

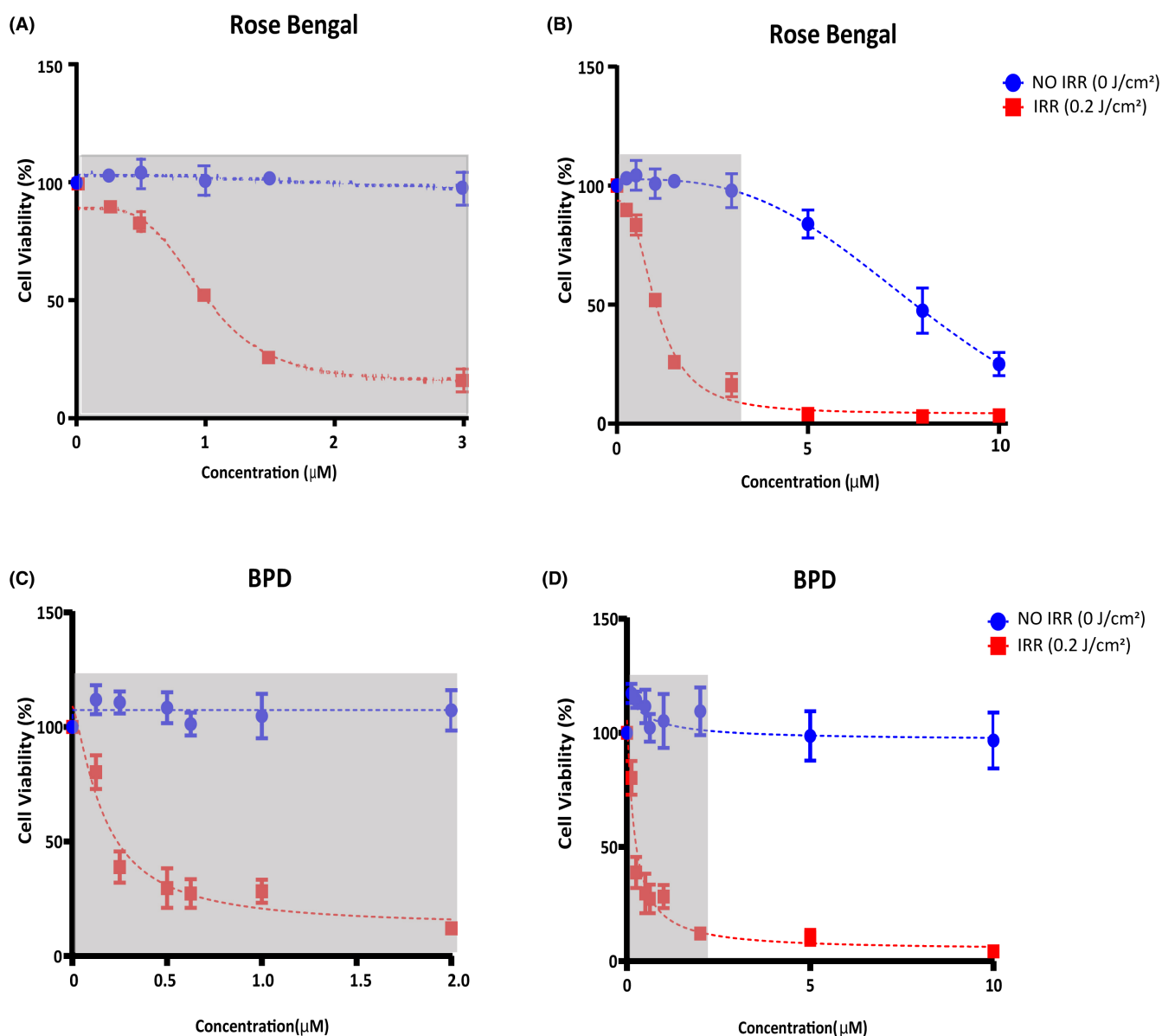


**FIGURE 5** Dose-response curves of positive controls. Rose bengal and BPD results for clinically relevant concentrations (shaded in gray) are shown in (A) and (C), respectively. Corresponding results for the OECD TG432 recommended range are shown in (B) and (D). The shaded region in the plots is a comparative representation of the clinically relevant 2× dose range of the test agent within the OECD recommend concentration range. All data points are average of three repeats. The error bars represent the standard error of mean (SEM). BPD, benzoporphyrin derivative; IRR, irradiation.

photocytotoxicity in a concentration-dependent manner. However, no non-irradiation toxicity was observed for BPD at the tested range.

Dose–response curves for tested fluorophores are shown in Figure 6. For fluorophores with strong absorption in the NIR range, namely, ICG and IRDye800, minimal changes in cell viability were observed at 2× clinical imaging concentration ranges and illumination parameters. IRDye800 products showed no significant decrease in cell viability at 1 and 6 J/cm<sup>2</sup>. For ICG, a modest decrease in cell viability (to 86%) was observed at 30 μM at 6 J/cm<sup>2</sup>. The cell viability plateaus to 39% in the 100–175 μM extended concentration range at 6 J/cm<sup>2</sup>, while no significant effect in cell viability is observed at 1 J/cm<sup>2</sup>. MB products at 1 J/cm<sup>2</sup> did not affect cell viability compared to NO IRR at the 2× clinical imaging concentration range. However, upon increasing the  $H_e$  to 6 J/cm<sup>2</sup>, significant photocytotoxicity was produced at concentrations between 5 and 30 μM. No significant difference between the NO IRR and IRR response curves was observed at concentrations above 60 μM. Proflavine products showed a significant decrease in cell viability at  $H_e$  as low as 0.6 J/cm<sup>2</sup>. The dose–response curve for proflavine appeared similar to those of positive controls and known RMS generators, BPD and RB. Proflavine at the 2× clinical imaging concentration range showed no change in cell viability upon increasing the concentration in the NO IRR group. However, a decrease in cell viability by almost 100% was observed for proflavine in the NO IRR group at higher concentrations (50–100 μM). In the case of MB and proflavine, significant inherent toxicity of the compounds was observed beside the irradiation effect in the expanded OECD concentration ranges, highlighting the light-dependent and light-independent cytotoxicity of the agents.

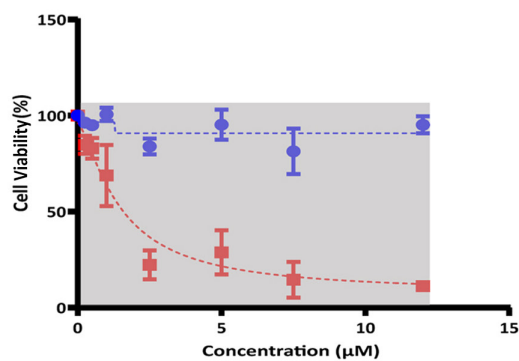
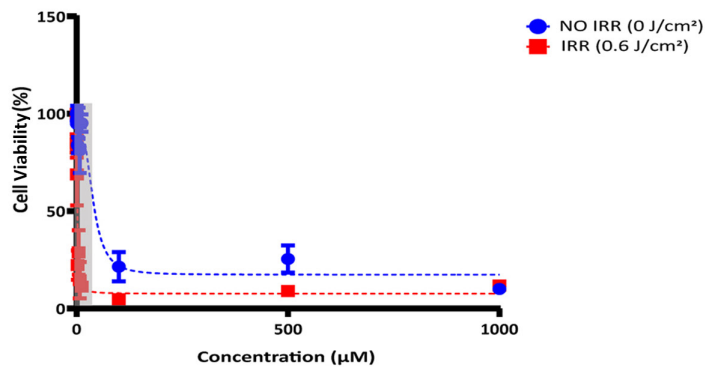
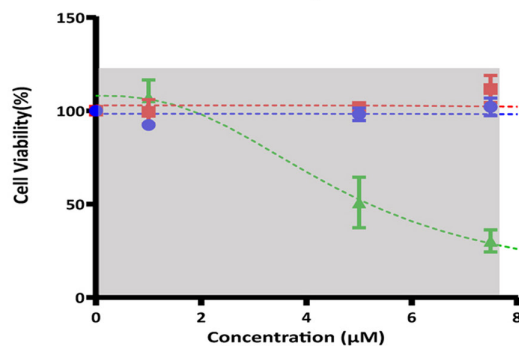
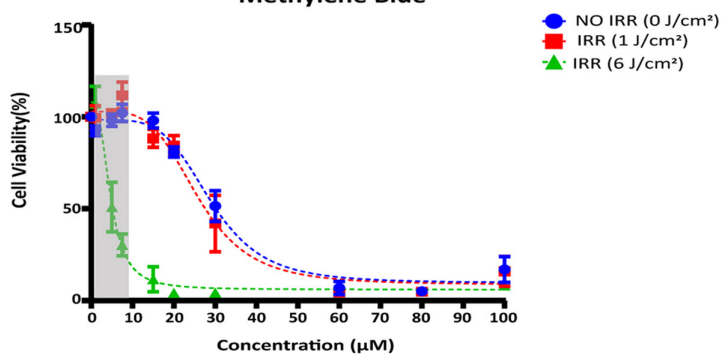
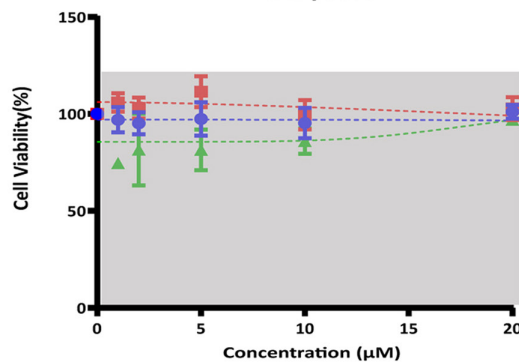
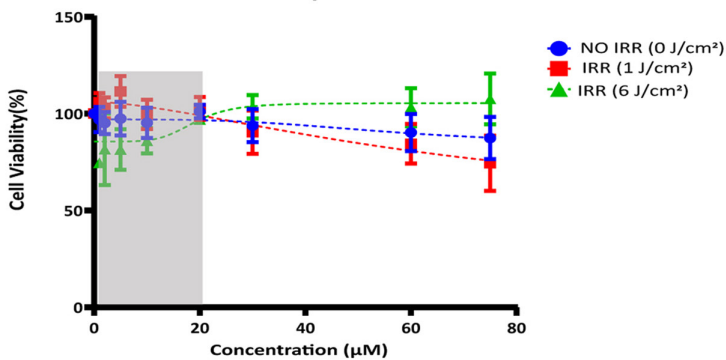
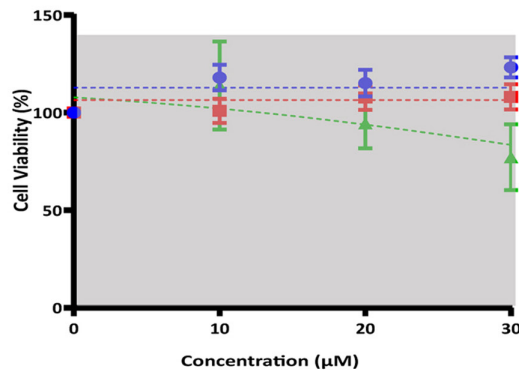
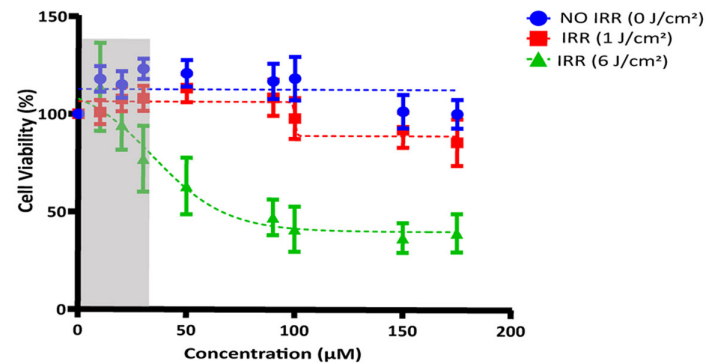
## MPE prediction model and data analysis

A tabular summary of the calculated MPE values for all the fluorophores at tested concentration ranges (2× clinical imaging concentration ranges and OECD extended concentration ranges) and illumination parameters is shown in Tables 3 and 4, respectively. Table 3 also compares the MPE values with the singlet oxygen production factor calculated at the 2× clinical imaging concentration ranges obtained from our previous cell-free study.<sup>56</sup> These results demonstrate the dependence of photocytotoxicity prediction on fluorophore type, concentration, and  $H_e$ . The dose–response curves for each fluorophore tested  $H_e$  was input into the phototox v.2 software to obtain MPE prediction model values using Equation (1). The results obtained from our previous study on the singlet-oxygen production by these agents showed substantial levels

of singlet-oxygen generation by RB and MB.<sup>56</sup> Other fluorophores—ICG, IRDye800, and proflavine—showed minimal singlet oxygen generation, while BPD was not tested previously. The fluorophore products can be categorized into three groups: phototoxic, non-phototoxic, and equivocal phototoxic, based on the MPE prediction model values (Equation 1) calculated from the dose–response curve summarized in Tables 3 and 4. Fluorophore products generated by known RMS generators—RB and BPD—were considered phototoxic at 2× clinical imaging and OECD extended concentration ranges as expected. IRDye800 products at 2× clinical imaging concentrations exhibited low photocytotoxicity at  $H_e$  1 J/cm<sup>2</sup>. IRDye800 illuminated at 6 J/cm<sup>2</sup> did not show any significant difference from the products generated at 1 J/cm<sup>2</sup> and thus was predicted to be non-phototoxic at all tested  $H_e$ . MB products exhibited no photocytotoxicity at J/cm<sup>2</sup> in the 2× clinical imaging concentration ranges. However, significant toxicity by MB was observed in the NO IRR group at extended OECD concentrations. An overlap in the NO IRR and IRR dose–response curves of MB at an extended OECD concentration range at 1 J/cm<sup>2</sup> was observed due to minimal IRR-based toxicity at the tested  $H_e$ . Hence, MB was predicted to be non-phototoxic due to minimal phototoxic effects in spite of significant inherent toxicity at the tested concentration range. At higher  $H_e$ , the MPE value depicts MB products as phototoxic or non-phototoxic at 2× clinical imaging and OECD extended concentration ranges, respectively. ICG at 2× clinical imaging concentration range was predicted to be non-phototoxic at 1 J/cm<sup>2</sup>. However, ICG products at an extended OECD concentration range were predicted to be equivocal phototoxic. At  $H_e$  of 6 J/cm<sup>2</sup>, ICG products were predicted to be phototoxic irrespective of the tested concentration range. Proflavine products were predicted to be phototoxic at  $H_e$  as low as 0.6 J/cm<sup>2</sup>, irrespective of the concentration range.

## DISCUSSION

Light-activated generation of RMS by a fluorescent agent is governed by various factors, such as excitation wavelength,  $H_e$ , irradiance, and the concentration of the contrast agent.<sup>57</sup> In this study, the goal was to identify optimal procedures and evaluate the utility of the test method for assessing the photocytotoxic potential of clinically used fluorescence imaging products using the NRU assay as indicated in OECD 432. Our results with the modified 3T3 NRU assay exhibited expected trends and predictions of photocytotoxicity for known phototoxic agents BPD and RB. BPD and RB showed a concentration-dependent decrease in cell viability at  $H_e$  as low as 0.2 J/cm<sup>2</sup>. RB is a

*2X Clinical imaging concentration range**Extended OECD concentration range (upto 100  $\mu\text{g/mL}$ )***(A) Proflavine****(B) Proflavine****(C) Methylene Blue****(D) Methylene Blue****(E) IRDye800****(F) IRDye800****(G) ICG****(H) ICG**



**FIGURE 6** Dose–response curves of test fluorophores from the NRU assay. Experimental results for (A and B) proflavine; (C and D) MB; (E and F) ICG; and (G and H) IRDye800 at clinically relevant concentrations (on the left) and irradiation wavelengths, as compared with OECD432-recommended testing concentration ranges of up to 100 µg/mL (on the right) for solar-radiation assessments. The shaded region in the plots is a comparative representation of the clinically relevant 2× dose range of the test agent within the OECD-recommended concentration range. IRR, irradiation; NRU, neutral red uptake.

**TABLE 3** Comparison of MPE prediction model values of singlet-oxygen (SO) production factor from the previous cell-free study calculated at clinical (2×) concentration range.

Fluorophore	Radiant exposure (J/cm <sup>2</sup> )	Conc. range-clinical (2×) (µM)	Excitation wavelength (nm)	MPE at clinical conc. range	Phototoxic prediction at 2× clinical conc. range	SO production factor [(F/H <sub>e</sub> )/µM] at 2× clinical conc. range (µM)
RB	0.2	0.5–3	520	0.344	Phototoxic	0.70 ± 0.001
BPD	0.2	0.5–2	685	0.701	Phototoxic	N/T (not tested)
ICG	1	1–30	785	0.075	Non-phototoxic	0.0012 ± 0.0002
	6	1–30	785	0.207	Phototoxic	
MB	1	1–7.5	660	0.041	Non-phototoxic	0.25 ± 0.01
	6	1–7.5	660	0.222	Phototoxic	
Proflavine	0.6	1–12	450	0.262	Phototoxic	0.0080 ± 0.0014
IRDye800	1	1–20	785	0.003	Non-phototoxic	0.0021 ± 0.00024
	6	1–20	785	0.005	Non-phototoxic	

Note: Interpretation of calculated MPE values based on the OECD TG 432: MPE <0.1 (No phototoxicity); MPE ≥0.1 and <0.15 (Equivocal phototoxicity); MPE ≥0.15 (Phototoxicity).

Abbreviations: BPD, benzoporphyrin derivative; ICG, indocyanine green; MB, methylene blue; MPE, mean photo effect; RB, rose bengal.

**TABLE 4** Tabular summary of the MPE prediction model values calculated at the OECD extended concentration ranges with optimized illumination parameter combinations for fluorophore products, using Phototox V.2. software.

Fluorophore	Radiant exposure (J/cm <sup>2</sup> )	Conc. range-OECD (µM)	Excitation wavelength (nm)	MPE at OECD conc. range	Phototoxic prediction at OECD conc. range
RB	0.2	0.5–10	520	0.424	Phototoxic
BPD	0.2	0.125–10	685	0.757	Phototoxic
ICG	1	1–175	785	0.113	Equivocal phototoxic
	6	1–175	785	0.538	Phototoxic
MB	1	1–500	660	0.079	Non-phototoxic
	6	1–500	660	0.305	Phototoxic
Proflavine	0.6	1–1000	450	0.294	Phototoxic
IRDye800	1	1–75	785	0.016	Non-phototoxic
	6	1–75	785	0.018	Non-phototoxic

Note: Interpretation of calculated MPE values based on the OECD TG 432: MPE <0.1 (No phototoxicity); MPE ≥0.1 and <0.15 (Equivocal phototoxicity); MPE ≥0.15 (Phototoxicity).

Abbreviations: BPD, benzoporphyrin derivative; ICG, indocyanine green; MB, methylene blue; MPE, mean photo effect; RB, rose bengal.

known singlet oxygen generator and has been reported to be used as an antimicrobial PDT agent.<sup>58</sup> BPD has been known to produce large quantities of RMS and is used as a photodynamic agent for treating age-related macular degeneration.<sup>59</sup> It is also worth noting that for agents like RB and BPD, with higher phototoxic potential,  $H_e$  as low as 0.2 J/cm<sup>2</sup> produced MPE prediction values in the

phototoxic range irrespective of the 2× clinical imaging concentration ranges and OECD extended concentration ranges. Given that significantly reduced cell viability is observed with BPD and RB at low light doses within the range of clinically used concentrations, these agents are undesirable for imaging purposes as phototoxicity is likely.

The dose–response curve of proflavine showed a trend similar to that of positive controls, BPD and RB. This trend was different from the results gathered in our previous study, where proflavine exhibited low singlet oxygen generation (Table 3).<sup>56</sup> The literature indicates that damage to cellular proteins by proflavine primarily involves superoxide ions and hydroxyl radicals.<sup>59–62</sup> Proflavine is a DNA-intercalating agent and accumulates in the nuclei. The overall photocytotoxicity observed in our *in vitro* test method could be due to the production of diverse RMS (singlet oxygen, hydroxyl radicals, and superoxide ions) generated by proflavine upon light activation. This apparent discrepancy between the results of our current and prior studies further highlights the need for phototoxicity screening with assays that can identify a range of mechanisms for photocytotoxic effects.

MB showed no significant change in cell viability in the 2× clinical concentration range at 1 J/cm<sup>2</sup>. However, cell viability was reduced to 50% in the presence of 6 J/cm<sup>2</sup> at 4.5 μM. The decrease in cell viability upon photoactivation can be correlated with a high amount of singlet oxygen generation at  $H_e$  of 6 J/cm<sup>2</sup> by MB reported in our previous study using a cell-free assay at the test illumination conditions (Table 3). However, the amount of singlet oxygen generated at 1 J/cm<sup>2</sup> was insufficient to cause a significant change in cell viability at the 2× clinical imaging concentration range. MB is also a known DNA intercalating agent<sup>63</sup> and has been shown to cause increased DNA damage in Barrett's esophagus after light activation during chromoendoscopy.<sup>64</sup> MB cytotoxicity at 30 μM was seen with and without irradiation. Thus, a concentration-dependent decrease in cell viability in the extended OECD concentration range for MB is likely a consequence of both phototoxicity and the inherent toxicity of the agent. Despite the clinical history of MB, our results and literature indicate that MB can generate phototoxicity due to potential RMS generation<sup>65</sup> and cause phototoxicity following MB-assisted imaging procedures.<sup>66–68</sup> Hence, it is critical to identify safe fluorophore concentrations and exposure levels for MB to be used safely for diagnostic imaging. Thus, prior literature appears to support the need for a phototoxicity testing regime that accounts for specific light and contrast agent dose levels.

IRDye800 showed no significant effect on cell viability at the tested concentration and illumination parameters in the study. The results obtained for IRDye800 with the modified approach are consistent with clinical trials demonstrating no adverse effects with the agent during clinical imaging procedures.<sup>15,45</sup> IRDye800 and ICG are mainly used as imaging agents and showed the lowest singlet oxygen generation potential at the tested 2× clinical imaging concentration range in our previous study. ICG is a commonly used dye for retinal angiography, evaluation

of cardiac output, and liver function, with a history of safety after intravenous administration.<sup>69,70</sup> ICG has low singlet oxygen quantum yield (0.077) and also showed low singlet oxygen generation potential in our previous study.<sup>56</sup> ICG dose–response curves at 1 and 6 J/cm<sup>2</sup> did not significantly change cell viability at 2× clinical concentrations. The cell viability plateaus at high testing concentrations (90–175 μM) as a function of  $H_e$ . A similar trend was observed with MCF-7 and HepG2 cell lines upon photoactivation of ICG in a prior study.<sup>71</sup> A previous study has shown that an increase in ICG concentration in an aqueous solution causes a decrease in the fluorescence intensity of the agent due to self-quenching effects.<sup>72</sup> Although ICG is FDA-approved as a contrast agent, it has also been explored in the literature as a photosensitizer at high light doses (50 mW/cm<sup>2</sup>, 785 nm LED light, 30 min) and concentrations.<sup>73</sup> Photosensitization of ICG produces singlet oxygen that rapidly oxidizes the agent leading to its decomposition into carbonyl compounds generated by cycloaddition of singlet oxygen.<sup>74</sup> ICG is also an effective light absorber for photothermal therapy applications.<sup>75,76</sup> It has been previously reported by Holzer et al. that most of the light energy absorbed by ICG is converted to heat by internal conversion.<sup>77</sup> Thus, the photocytotoxic effect of ICG observed in our study could be due to a combination of RMS generation and photothermal effects. Additional support for our results from the modified NRU assay approach comes from the MPE prediction model values calculated using the Phototox software and the main use of these fluorophores. The MPE prediction model is based on a comparison of the complete concentration–response curves obtained at the tested concentrations and  $H_e$  combinations. An MPE can be calculated within a concentration range where at least one of the dose–response curves (NO IRR or IRR) still exhibits at least 10% response.

The methods implemented in this study deviate from standard approaches in that they focus on generating results for clinically relevant light and agent doses. This approach may enable the same contrast agent to be used for imaging and phototherapy, depending on concentration and illumination. Additionally, evaluating overall photocytotoxicity produced using the *in vitro* 3T3 NRU assay may help determine a safe concentration and illumination dose range for clinical imaging. The proposed methods will facilitate the development of innovative diagnostic technologies that are safe for clinical use and benefit public health. Results from this study also represent critical scientific information that may provide direction toward establishing consensus standards for contrast-enhanced fluorescent imaging products.

Although there is generally good agreement between our experimental results and the literature, there are some issues with the NRU approach. The premise underlying

this assay is that a cytotoxic chemical interferes with normal lysosomal uptake, representing the number of viable cells. Intact lysosomal integrity is only maintained in viable cells.<sup>78</sup> The degree of cell viability inhibition and associated phototoxicity for an agent would be affected by the concentration of the test agent used, inherent cytotoxicity of the agent without irradiation, and the RMS generated at given illumination parameters. The solubility of the test agent in the solvent (Table S1) and cell media should also be taken into consideration since hydrophobic contrast agents can aggregate at higher concentrations which might affect the cell viability upon photoactivation. Additionally, any test agent having a localized effect on the lysosomes will result in low cell number and reduced viability. The induction of precipitation of the neutral dye by some chemical agents might also impact the accuracy of the absorbance readings used to detect NR uptake.<sup>79,80</sup>

The current modified in vitro approach, although robust in capturing the overall effect of photoactivation of a fluorophore, is not informative in determining the mechanism of action of phototoxicity. Our previous study used a cell-free assay to quantify singlet oxygen produced by contrast-enhanced fluorescence imaging agents.<sup>56</sup> This produced essential information about a potential phototoxicity mechanism of interest for the tested fluorophores. Together, the cell-free and the in vitro phototoxicity assessment strategies could constitute an informative test methodology to evaluate the potential phototoxicity of emerging fluorescence imaging products. Based on our current and previous results, the phototoxicity testing of fluorescence imaging products should include initial testing with the cell-free and the in vitro phototoxicity assessment strategy. While the modified NRU assay would help evaluate the biological effects caused by the test fluorophore products, the cell-free assay will provide a better understanding of the RMS involved in associated phototoxicity upon photoactivation. Our future work will focus on (1) developing test methods that can be standardized to quantify other RMS (hydroxyl radicals, superoxide ions, etc.) generated by fluorescent contrast agents and (2) in vivo test methods to detect RMS generation and associated photocytotoxicity of fluorescence contrast agents used for diagnostic purposes.

## CONCLUSION

In this study, we have proposed and evaluated a modified in vitro method based on the neutral red uptake assay (NRU) for assessing the photocytotoxicity of fluorescence products generated under clinical conditions. Results obtained from this study align well with our recent work on reactive oxygen species generation with a cell-free assay and prior published results on in vivo phototoxic effects

of fluorophores. Therefore, this approach may represent a practical and least burdensome approach for phototoxicity screening of emerging visible to near-infrared fluorescence imaging products.

## ACKNOWLEDGMENTS

This work is supported by the NSF-FDA scholar-in-residence Program CBET-2037815. Ms. Shruti Vig is supported by the MPower Fellowship. Mr. Brandon Gaitan is supported by the Clark Doctoral Fellowship. Mr. Lucas Frankle is supported by the University of Maryland ASPIRE Fellowship.

## DISCLAIMER

The mention of commercial products, their sources, or their use in connection with material reported herein is not to be construed as an actual or implied endorsement of such products by the Department of Health and Human Services.

## ORCID

Shruti Vig  <https://orcid.org/0000-0002-0534-1571>

Huang-Chiao Huang  <https://orcid.org/0000-0002-5406-0733>

## REFERENCES

1. Tipirneni KE, Rosenthal EL, Moore LS, et al. Fluorescence imaging for cancer screening and surveillance. *Mol Imaging Biol*. 2017;19(5):645-655.
2. Stummer W, Suero Molina E. Fluorescence imaging/agents in tumor resection. *Neurosurg Clin N Am*. 2017;28(4):569-583.
3. Pierce MC, Javier DJ, Richards-Kortum R. Optical contrast agents and imaging systems for detection and diagnosis of cancer. *Int J Cancer*. 2008;123(9):1979-1990.
4. Yamamoto M. Indocyanine green angiography for intraoperative assessment in vascular surgery. *Eur J Vasc Endovasc Surg*. 2012;43(4):426-432.
5. Brancato R, Bandello F, Lattanzio R. Iris fluorescein angiography in clinical practice. *Surv Ophthalmol*. 1997;42(1):41-70.
6. Vahrmeijer AL. Image-guided cancer surgery using near-infrared fluorescence. *Nat Rev Clin Oncol*. 2013;10(9):507-518.
7. Palmieri G, Cofano F, Salvati LF, et al. Fluorescence-guided surgery for high-grade gliomas: state of the art and new perspectives. *Technol Cancer Res Treat*. 2021;20:1-11.
8. Polom W, Markuszewski M, Rho YS, Matuszewski M. Use of invisible near-infrared light fluorescence with indocyanine green and methylene blue in urology. Part 2. *Cent Eur J Urol*. 2014;67(3):310-313.
9. van Manen L, Handgraaf HJM, Diana M, et al. A practical guide for the use of indocyanine green and methylene blue in fluorescence-guided abdominal surgery. *J Surg Oncol*. 2018;118(2):283-300.
10. Tummers QR, Verbeek FP, Schaafsma BE, et al. Real-time intraoperative detection of breast cancer using near-infrared fluorescence imaging and methylene blue. *Eur J Surg Oncol*. 2014;40(7):850-858.

11. van der Vorst JR, Schaafsma BE, Verbeek FP, et al. Intraoperative near-infrared fluorescence imaging of parathyroid adenomas with use of low-dose methylene blue. *Head Neck*. 2014;36(6):853-858.
12. Cwalinski T, Polom W, Marano L, et al. Methylene blue—current knowledge, fluorescent properties, and its future use. *J Clin Med*. 2020;9(11):35-38.
13. Varghese P, Abdel-Rahman AT, Akberali S, Mostafa A, Gattuso JM, Carpenter R. Methylene blue dye—a safe and effective alternative for sentinel lymph node localization. *Breast J*. 2008;14(1):61-67.
14. Kawedia JD, Zhang YP, Myers AL, et al. Physical and chemical stability of proflavine contrast agent solutions for early detection of oral cancer. *J Oncol Pharm Pract*. 2016;22(1):21-25.
15. Rosenthal EL, Warram JM, de Boer E, et al. Safety and tumor specificity of cetuximab-IRDye800 for surgical navigation in head and neck cancer. *Clin Cancer Res*. 2015;21(16):3658-3666.
16. Hernot S, van Manen L, Debie P, Mieog JSD, Vahrmeijer AL. Latest developments in molecular tracers for fluorescence image-guided cancer surgery. *Lancet Oncol*. 2019;20(7):e354-e367.
17. Feasibility trial for real-time identification of the ureters with a methylene-blue. NCT05111808. November 8, 2021. Accessed April 24, 2023. <https://clinicaltrials.gov/show/NCT05111808>
18. Fluorescent imaging and methylene blue: ureter study. NCT03177070. June 6, 2017. <https://clinicaltrials.gov/show/NCT03177070>
19. Intra-operative infra-red fluorescent imaging in thyroid and parathyroid surgery. NCT02089542. March 17, 2014. Accessed April 24, 2023. <https://clinicaltrials.gov/show/NCT02089542>
20. Near infrared fluorescent imaging in thyroid and parathyroid surgery with the Fluobeam (TM) system of Fluoptics. NCT01598727. May 15, 2012. Accessed April 24, 2023. <https://clinicaltrials.gov/ct2/show/NCT01598727>
21. COVID-19 treatment using methylene blue and photodynamic therapy. NCT04933864. June 22, 2021. Accessed June 16, 2023. <https://clinicaltrials.gov/show/NCT04933864>
22. Efficacy of methylene blue mediated photodynamic therapy for primary localized cutaneous amyloidosis treatment in Asians. NCT03068208. March 1, 2017. Accessed June 16, 2023. <https://clinicaltrials.gov/show/NCT03068208>
23. Comparison of efficacy and safety between methylene blue-mediated photodynamic therapy and 5% amorolfine nail lacquer for toenail onychomycosis treatment. NCT03098342. March 31, 2017. Accessed June 16, 2023. <https://clinicaltrials.gov/show/NCT03098342>
24. King Saud U. ICG-PDT, periimplantitis, diabetes mellitus. NCT04833569. April 6, 2021. Accessed June 16, 2023. <https://clinicaltrials.gov/show/NCT04833569>
25. Single session of antimicrobial photodynamic therapy using indocyanine green. NCT02043340. January 23, 2014 (CTG Labs—NCBI).
26. Center for Devices and Radiological Health, FDA. Laser products—conformance with IEC 60825–1 Ed. 3 and IEC 60601–2-22 Ed. 3.1 (Laser Notice No. 56). 2019. Accessed December 22, 2022. <https://www.fda.gov/media/110120/download>
27. International Electrotechnical Commission (IEC). Photobiological safety of lamps and lamp systems, IEC 62471:Ed. 1.0: 2006. 2006–2007. 2006. Accessed January 9, 2023. <https://webstore.iec.ch/publication/7076>
28. Khandpur S, Porter RM, Boulton SJ, Anstey A. Drug-induced photosensitivity: new insights into pathomechanisms and clinical variation through basic and applied science. *Br J Dermatol*. 2017;176(4):902-909.
29. Kim K, Park H, Lim KM. Phototoxicity: its mechanism and animal alternative test methods. *Toxicol Res*. 2015;31(2):97-104.
30. Baptista MS, Cadet J, Di Mascio P, et al. Type I and type II photosensitized oxidation reactions: guidelines and mechanistic pathways. *Photochem Photobiol*. 2017;93(4):912-919.
31. Borenfreund E, Puerner JA. Toxicity determined in vitro by morphological alterations and neutral red absorption. *Toxicol Lett*. 1985;24(2):119-124.
32. Bulychiev A, Trouet A, Tulkens P. Uptake and intracellular distribution of neutral red in cultured fibroblasts. *Exp Cell Res*. 1978;115(2):343-355.
33. Thorne D, Wiecezorek R, Fukushima T. A survey of aerosol exposure systems relative to the analysis of cytotoxicity: a Cooperation Centre for Scientific Research Relative to Tobacco (CORESTA) perspective. *Toxicol Res Appl*. 2021;5:239784732110222.
34. Borenfreund E, Puerner JA. A simple quantitative procedure using monolayer cultures for cytotoxicity assays (HTD/NR-90). *J Tissue Cult Methods*. 1985;9(1):7-9.
35. Lynch AM, Wilcox P. Review of the performance of the 3T3 NRU in vitro phototoxicity assay in the pharmaceutical industry. *Exp Toxicol Pathol*. 2011;63(3):209-214.
36. Ceridono M, Tellner P, Bauer D, et al. The 3T3 neutral red uptake phototoxicity test: practical experience and implications for phototoxicity testing—the report of an ECVAM-EFPIA workshop. *Regul Toxicol Pharmacol*. 2012;63(3):480-488.
37. OECD. Test No. 432: In Vitro 3T3 NRU Phototoxicity Test, OECD Guidelines for the Testing of Chemicals, Section 4. OECD Publishing; 2019. doi:10.1787/9789264071162-en
38. Prieto Peraita M, Griesinger C, Amcoff S, Whelan M. EURL ECVAM Recommendation on the 3T3 Neutral Red Uptake Cytotoxicity Assay for Acute Oral Toxicity Testing. Publications Office of the European Union; 2013 (JRC79556).
39. FDA. S10 photosafety evaluation of pharmaceuticals. 2015. Accessed January 9, 2023. <https://www.fda.gov/media/85076/download>
40. Verbeek FPR, van der Vorst JR, Schaafsma BE, et al. Intraoperative near infrared fluorescence guided identification of the ureters using low dose methylene blue: a first in human experience. *J Urol*. 2013;190(2):574-579.
41. Tagaya N, Yamazaki R, Nakagawa A, et al. Intraoperative identification of sentinel lymph nodes by near-infrared fluorescence imaging in patients with breast cancer. *Am J Surg*. 2008;195(6):850-853.
42. Zhu B, Seveck-Muraca EM. A review of the performance of near-infrared fluorescence imaging devices used in clinical studies. *Br J Radiol*. 2015;88(1045):20140547.
43. Di Stefano AFD, Radicioni MM, Vaccani A, et al. Methylene blue MMX® tablets for chromoendoscopy. Bioavailability, colon staining and safety in healthy volunteers undergoing a full colonoscopy. *Contemp Clin Trials*. 2018;71:96-102.
44. Matsui A, Tanaka E, Choi HS, et al. Real-time, near-infrared, fluorescence-guided identification of the ureters using methylene blue. *Surgery*. 2010;148(1):78-86.



45. Miller SE, Tummers WS, Teraphongphom N, et al. First-in-human intraoperative near-infrared fluorescence imaging of glioblastoma using cetuximab-IRDye800. *J Neurooncol*. 2018;139(1):135-143.
46. Dsouza AV, Lin H, Henderson ER, Samkoe KS, Pogue BW. Review of fluorescence-guided surgery systems: identification of key performance capabilities beyond indocyanine green imaging. *J Biomed Opt*. 2016;21(8):080901.
47. Tang Y, Carns J, Polydorides AD, Anandasabapathy S, Richards-Kortum RR. In vivo white light and contrast-enhanced vital-dye fluorescence imaging of Barrett's-related neoplasia in a single-endoscopic insertion. *J Biomed Opt*. 2016;21(8):086004.
48. Shin D, Pierce MC, Gillenwater AM, Williams MD, Richards-Kortum RR. A fiber-optic fluorescence microscope using a consumer-grade digital camera for in vivo cellular imaging. *PLoS ONE*. 2010;5(6):e11218.
49. Pérez-Laguna V, García-Luque I, Ballesta S, et al. Antimicrobial photodynamic activity of rose bengal, alone or in combination with Gentamicin, against planktonic and biofilm *Staphylococcus aureus*. *Photodiagnosis Photodyn Ther*. 2018;21:211-216.
50. Fingar VH, Kik PK, Haydon PS, et al. Analysis of acute vascular damage after photodynamic therapy using benzoporphyrin derivative (BPD). *Br J Cancer*. 1999;79(11):1702-1708.
51. Tsoukas MM, Lin GC, Lee MS, Anderson RR, Kollias N. Predictive dosimetry for threshold phototoxicity in photodynamic therapy on normal skin: red wavelengths produce more extensive damage than blue at equal threshold doses. *J Invest Dermatol*. 1997;108(4):501-505.
52. Repetto G, del Peso A, Zurita JL. Neutral red uptake assay for the estimation of cell viability/cytotoxicity. *Nat Protoc*. 2008;3(7):1125-1131.
53. Holzhütter H-G. A general measure of in vitro phototoxicity derived from pairs of dose-response curves and its use for predicting the in vivo phototoxicity of chemicals. *Altern Lab Anim*. 1997;25(4):445-462.
54. Spielmann H, Balls M, Dupuis J, et al. The international EU/COLIPA In vitro phototoxicity validation study: results of phase II (blind trial). Part 1: the 3T3 NRU phototoxicity test. *Toxicol In Vitro*. 1998;12(3):305-327.
55. Goulart Rde C, Boleam M, Tde Paulino P, et al. Photodynamic therapy in planktonic and biofilm cultures of *Aggregatibacter actinomycetemcomitans*. *Photomed Laser Surg*. 2010;28(Suppl 1):S53-S60.
56. Gaitan B, Frankle L, Vig S, et al. Quantifying the photochemical damage potential of contrast-enhanced fluorescence imaging products: singlet oxygen production. *Photochem Photobiol*. 2022;98(4):736-747.
57. De Silva P, Saad MA, Thomsen H, Bano S, Ashraf S, Hasan T. Photodynamic therapy, priming and optical imaging: potential co-conspirators in treatment design and optimization—a Thomas Dougherty Award for Excellence in PDT paper. *J Porphyr Phthalocyanines*. 2020;24:1320-1360.
58. Arboleda A, Miller D, Cabot F, et al. Assessment of rose bengal versus riboflavin photodynamic therapy for inhibition of fungal keratitis isolates. *Am J Ophthalmol*. 2014;158(1):64-70.e2.
59. Kramer M, Miller JW, Michaud N, et al. Liposomal benzoporphyrin derivative verteporfin photodynamic therapy: selective treatment of choroidal neovascularization in monkeys. *Ophthalmology*. 1996;103(3):427-438.
60. Gatasheh MK, Malik A, Ola MS, Alhomida AS. Photo-activated proflavine degrades protein and impairs enzyme activity: involvement of hydroxyl radicals. *Toxicol Rep*. 2022;9:78-86.
61. Piette J, Decuyper J, Machiroux R, Calberg-Bacq CM, van de Vorst A, Lion Y. Visible-light-induced OH radicals in DNA-proflavine complexes: an e.p.r. and spin trapping study. *Int J Radiat Biol Relat Stud Phys Chem Med*. 1982;42(2):151-161.
62. Gatasheh MKM, Subbaram K, Kannan H, Naseem I. Generation of oxygen free radicals by proflavine: implication in protein degradation. *HAYATI J Biosci*. 2017;24(3):118-123.
63. Bradley DF, Stellwagen NC, O'Konski CT, Paulson CM. Electric birefringence and dichroism of acridine orange and methylene blue complexes with polynucleotides. *Biopolymers*. 1972;11(3):645-652.
64. Olliver JR, Wild CP, Sahay P, Dexter S, Hardie LJ. Chromoendoscopy with methylene blue and associated DNA damage in Barrett's esophagus. *Lancet*. 2003;362(9381):373-374.
65. Epe B, Hegler J, Wild D. Singlet oxygen as an ultimately reactive species in *Salmonella typhimurium* DNA damage induced by methylene blue/visible light. *Carcinogenesis*. 1989;10(11):2019-2024.
66. Kluk J, Charles-Holmes R, Markham D. Acute phototoxicity induced by methylene blue-assisted parathyroidectomy: an unreported risk of a common procedure. *Br J Dermatol*. 2012;166(4):907-908.
67. Lambrecht P, Vandeplas G, van Slycke S, Smet PF, Brusselsaers N, Vermeersch H. Phototoxic reaction after parathyroid surgery: case report and review of the literature. *Acta Clin Belg*. 2012;67(6):438-441.
68. Maguire CA, Sharma A, Alarcon L, et al. Histological features of methylene blue-induced phototoxicity administered in the context of parathyroid surgery. *Am J Dermatopathol*. 2017;39(8):e110-e115.
69. Alander JT, Kaartinen I, Laakso A, et al. A review of indocyanine green fluorescent imaging in surgery. *Int J Biomed Imaging*. 2012;2012:940585.
70. Boni L, David G, Mangano A, et al. Clinical applications of indocyanine green (ICG) enhanced fluorescence in laparoscopic surgery. *Surg Endosc*. 2015;29(7):2046-2055.
71. El-Daly SM, Gamal-Eldeen AM, Abo-Zeid MA, Borai IH, Wafay HA, Abdel-Ghaffar AR. Photodynamic therapeutic activity of indocyanine green entrapped in polymeric nanoparticles. *Photodiagnosis Photodyn Ther*. 2013;10(2):173-185.
72. Saxena V, Sadoqi M, Shao J. Degradation kinetics of indocyanine green in aqueous solution. *J Pharm Sci*. 2003;92(10):2090-2097.
73. Lim H-J, Oh CH. Indocyanine green-based photodynamic therapy with 785nm light emitting diode for oral squamous cancer cells. *Photodiagnosis Photodyn Ther*. 2011;8(4):337-342.
74. Engel E, Schraml R, Maisch T, et al. Light-induced decomposition of indocyanine green. *Invest Ophthalmol Vis Sci*. 2008;49(5):1777-1783.
75. Shirata C, Kaneko J, Inagaki Y, et al. Near-infrared photothermal/photodynamic therapy with indocyanine green induces apoptosis of hepatocellular carcinoma cells through oxidative stress. *Sci Rep*. 2017;7(1):13958.
76. Zheng X, Zhou F, Wu B, Chen WR, Xing D. Enhanced tumor treatment using biofunctional indocyanine green-containing nanostructure by intratumoral or intravenous injection. *Mol Pharm*. 2012;9(3):514-522.

77. Holzer W, Mauere M, Penzkofer A, et al. Photostability and thermal stability of indocyanine green. *Photochem Photobiol.* 1998;47(2):155-164.
78. Wang F, Gómez-Sintes R, Boya P. Lysosomal membrane permeabilization and cell death. *Traffic.* 2018;19(12):918-931.
79. Barile FA. 3—Continuous cell lines as a model for drug toxicity assessment. In: Castell JV, Gmez-Lechn MJ, eds. *In Vitro Methods in Pharmaceutical Research.* Academic Press; 1997:33-54.
80. McGaw LJ, Elgorashi EE, Eloff JN. 8—Cytotoxicity of African Medicinal Plants Against Normal Animal and Human Cells, *Toxicological Survey of African Medicinal Plants.* Elsevier; 2014:181-233.
81. Unno N, Inuzuka K, Suzuki M, et al. Preliminary experience with a novel fluorescence lymphography using indocyanine green in patients with secondary lymphedema. *J Vasc Surg.* 2007;45(5):1016-1021.
82. Takeuchi M, Sugie T, Abdelazeem K, et al. Lymphatic mapping with fluorescence navigation using indocyanine green and axillary surgery in patients with primary breast cancer. *Breast J.* 2012;18(6):535-541.
83. Imai T, Takahashi K, Goto F, Morishita Y. Measurement of blood concentration of indocyanine green by pulse dye densitometry—comparison with the conventional spectrophotometric method. *J Clin Monit Comput.* 1998;14(7-8):477-484.
84. Gao RW, Teraphongphom N, de Boer E, et al. Safety of panitumumab-IRDye800CW and cetuximab-IRDye800CW for fluorescence-guided surgical navigation in head and neck cancers. *Theranostics.* 2018;8(9):2488-2495.
85. Wide-field and high-resolution in vivo imaging in visualizing lesions in patients with oral neoplasia undergoing surgery. NCT012699190. December 30, 2010. Accessed April 24, 2023. <https://clinicaltrials.gov/show/NCT01269190>

## SUPPORTING INFORMATION

Additional supporting information can be found online in the Supporting Information section at the end of this article.

**How to cite this article:** Vig S, Gaitan B, Frankle L, et al. Test method for evaluating the photocytotoxic potential of fluorescence imaging products. *Photochem Photobiol.* 2023;00:1-18. doi:[10.1111/php.13836](https://doi.org/10.1111/php.13836)